

ARTICLE OPEN



Drivers of accelerated warming in Mediterranean climate-type regions

Diego Urdiales-Flores¹, George Zittis¹✉, Panos Hadjinicolaou¹, Sergey Osipov^{2,3}, Klaus Klingmüller³, Nikos Mihalopoulos^{1,4,5}, Maria Kanakidou^{5,6}, Theo Economou¹ and Jos Lelieveld^{1,3}✉

The near-surface temperature in Mediterranean climate-type regions has increased overall similarly or more rapidly than the global mean rates. Although these regions have comparable climate characteristics and are located at similar latitudes, recent warming acceleration is most pronounced in the Mediterranean Basin. Here, we investigate the contributions of several climate drivers to regional warming anomalies. We consider greenhouse gases, aerosols, solar irradiance, land–atmosphere interactions, and natural climate variability modes. Our results highlight the dominant role of anthropogenic greenhouse gas radiative forcing in all Mediterranean climate-type regions, particularly those in the northern hemisphere. In the Mediterranean Basin, the recent warming acceleration is largely due to the combined effect of declining aerosols and a negative trend in near-surface soil moisture. While land–atmosphere feedbacks are also important in other locations (e.g., California and Southern Africa), this synergy is unique in the Mediterranean Basin. These two regional climate drivers have natural and anthropogenic components of equivalent importance. Such feedbacks are not fully resolved in the current regional climate projections.

npj Climate and Atmospheric Science (2023)6:97; <https://doi.org/10.1038/s41612-023-00423-1>

INTRODUCTION

Mediterranean climate-type regions (MCRs) are defined by temperate, wet winters and warm to hot, dry summers¹. They are typically found at the western edges of continents, in coastal locations, and are determined by the geography of winter storm tracks and summer subtropical anticyclones. In the widely used Köppen–Geiger classification (see Methods), these regimes are described as temperate summer-dry, which translates into natural vegetation types of sparse woodlands, grasses, and shrubs that may have been converted into agricultural land^{2,3}. Besides the Mediterranean Basin (MED), mainly the northern part, such climate zones are found in North America—California (NAC), South America—Central Chile (SAC), parts of Southern Africa (SAF), and Southern Australia (SAU). These climate zones currently encompass only 2% of the Earth's land surface (Supplementary Fig. 1), while their total population is estimated at more than 700 million inhabitants or ~10% of the global population. Due to their characteristic temperate and summer-dry environments, they are considered to be biodiversity hot spots for which conservation is of high priority^{4,5}.

Following the global trends, MCRs have significantly warmed during the last century^{6–9}. Particularly in the Mediterranean Basin, the warming has accelerated in the past four decades, exceeding the global average rates^{7,10,11}, which is most striking in the eastern part of the Basin¹². A less robust transition to drier conditions has also been identified^{12–21}. A profound increase in the intensity of heat extremes has been observed and is attributed to anthropogenic activities (medium-to-high confidence)²². However, there is less confidence in the analyses of precipitation changes and associated extremes (including the occurrence of agricultural/ecological droughts), except for the Mediterranean Basin, for which there is low-to-medium confidence in the human

contribution²². These regional warming and drying trends are expected to continue in the 21st century and beyond^{8,9,12,23–27}. Owing to the shifts in the mean values and variability of temperature and precipitation, as well as robust changes in the large-scale, upper-tropospheric flow and the reduction in regional land–sea temperature gradients during the winter, the Mediterranean Basin is recognized as a prominent global climate change hot spot^{28,29}. The latter feedback (reduction of land–sea temperature gradients during winter) contributes to a wet-season precipitation decline that contributes to the region's disproportionate climate change impacts²⁹.

Temperature variability depends on several global or regional drivers, such as changes in solar activity and incoming irradiance, radiative forcing from natural and anthropogenic greenhouse gases (GHGs), large-scale volcanic eruptions, modes of internal climate variability, such as the El Niño–Southern Oscillation (ENSO), and more local features such as the presence of mineral dust and aerosol pollution, land–atmosphere interactions or extensive land-use changes such as urbanization and deforestation^{30–38}. Despite the differences in responses on the regional scale, these climate variability drivers and their relative contributions to the observed trends have, so far, been explored primarily on global or continental scales^{35,39–42}.

Here, we present an updated assessment of historical temperature trends in the various Mediterranean climate-type zones around the globe. Our primary objective is to understand why, particularly since the 1980s, the Mediterranean Basin (mainly its eastern part) has been warming significantly more rapidly than the global average rates and other regions of similar climatic characteristics within the same latitudinal zone. Further, we identify and highlight the dominant drivers of temperature variability and quantify their contribution to each MCR.

¹Climate and Atmosphere Research Center (CARE-C), The Cyprus Institute, Nicosia, Cyprus. ²King Abdullah University of Science and Technology (KAUST), Thuwal, Saudi Arabia. ³Department of Atmospheric Chemistry, Max Planck Institute for Chemistry, Mainz, Germany. ⁴Institute for Environmental Research and Sustainable Development, National Observatory of Athens, Athens, Greece. ⁵Environmental Chemical Processes Laboratory (ECPL), Department of Chemistry, University of Crete, Heraklion, Greece. ⁶Institute of Environmental Physics, University of Bremen, Bremen, Germany. ✉email: g.zittis@cyi.ac.cy; jos.lelieveld@mpic.de

RESULTS

Recent warming acceleration in MCRs

The observed (land-only) global and MCR near-surface air temperature trends of the last 120 years (1901–2020) are presented in the top panel of Fig. 1. Considering the entire time series, MCRs have warmed at a similar pace as the global average (~ 0.11 °C/decade). One exception is in the SAC region in Chile, where the historical warming rate is nearly half as high (0.06 °C/decade). However, since the beginning of the 1980s, regional warming has accelerated. Particularly the Mediterranean Basin (MED) is warming overall more rapidly than the global mean rates and other MCRs (Fig. 1—bottom panel). In this region, the median trend for 1981–2020 exceeds 0.4 °C/decade, almost 1.5 times the global average over land (0.28 °C/decade). In addition to the spatial gradients, the statistical significance of trends also varies between the different MCRs (not shown). The warming rate in the SAC region of Chile continues to be the lowest among all areas under investigation, next to Southern Australia (SAU), which has not experienced a recent acceleration.

Relative contribution of temperature drivers

To identify the main causes of recent warming trends (1981–2020) and quantify the association and relative contributions of five climate drivers to the observed temperature variability, we utilize

the well-established framework of multivariate lagged linear regression (see Methods). In particular, the parameters included in this analysis are (i) the radiative forcing from well-mixed Greenhouse Gases (WMGHG), (ii) the Total Solar Irradiance (TSI), (iii) the column Aerosol Optical Depth (AOD) in the visible spectrum, including both anthropogenic and natural components, (iv) the near-surface soil moisture (SM), and (v) the Multivariate El Niño/Southern Oscillation Index (MEI). The multivariate lagged linear regression model also allows interactions between the five major climate drivers (predictors). AOD and SM are derived from the MERRA-2 and ERA5 reanalysis, respectively, while the other parameters are observation-based (see Methods).

In all regions with Mediterranean climate characteristics, the model captures most of the observed variance during the last four decades (74–90%) (Fig. 2). This is also the case for the warming rates, which are, however, slightly underestimated (Table 1). The confidence intervals (interquartile range) based on bootstrap resampling (see Methods) are also provided in the whiskers of Fig. 2 and Supplementary Table 1. According to our estimations, a small part of the observed variability remains unexplained by the selected drivers. This fraction ranges from 12 to 26%, with the highest percentage in South America—Central Chile (SAC).

The contribution of increasing greenhouse gases (see also Supplementary Fig. 2) is predominant in all regions, explaining

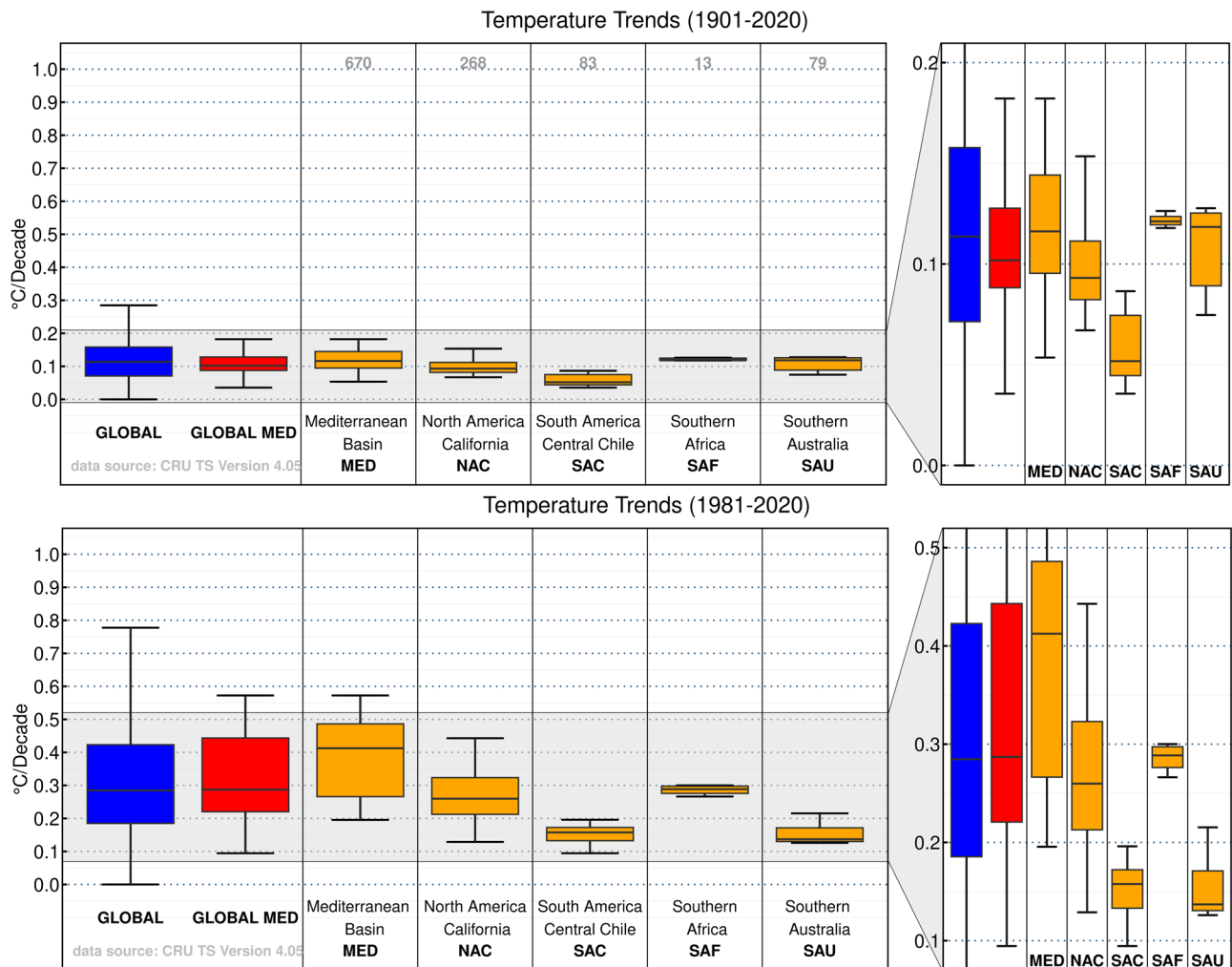


Fig. 1 Observed global and regional temperature trends (land-only) for the different Mediterranean climate-type regions for 1901–2020 (top panel) and 1981–2020 (bottom panel). GLOBAL MED represents all Mediterranean climate-type regions. The number of grid cells of each Mediterranean climate-type region is indicated. Boxes represent the interquartile range; whiskers represent the range spanned by the individual temperature trends across the grid cells of each region.

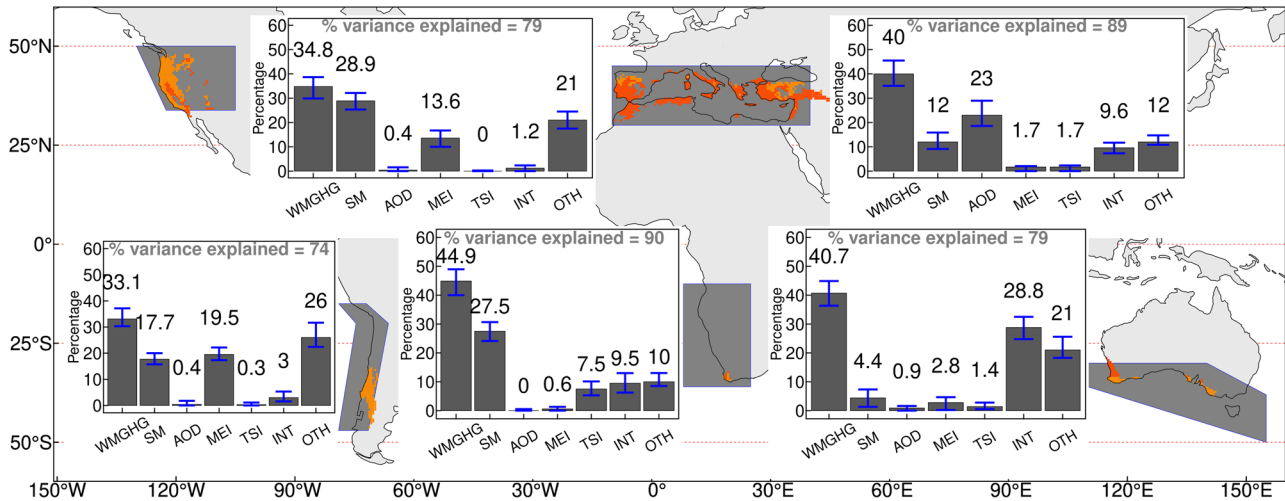


Fig. 2 Relative contribution of temperature drivers. Relative contributions of five main drivers in the Mediterranean climate-type regions (dry summer climate zones with hot summers—Csa in red, and warm summer conditions—Csb in orange) for 1981–2020 to the observed near-surface temperature variability (WMGHG well-mixed greenhouse gases radiative forcing, SM near-surface soil moisture, AOD aerosol optical depth, MEI Multivariate El Niño/Southern Oscillation Index, TSI total solar irradiance, INT interactions among drivers, OTH other drivers). Whiskers represent confidence intervals (interquartile range) based on bootstrap resampling (1000 iterations). The IPCC Working Group I regions that include Mediterranean climate-type regimes are gray-shaded for reference.

Table 1. Observed and reconstructed (model) regional temperature trends (1981–2020) attributed to five climate drivers.

Temperature trend	MED	NAC	SAC	SAF	SAU
WMGHG	0.181 ± 0.0009	0.161 ± 0.0008	0.076 ± 0.0003	0.133 ± 0.0006	0.098 ± 0.0004
AOD	0.103 ± 0.0013	0.003 ± 0.0001	0.001 ± 0.0001	0.001 ± 0.0003	0.009 ± 0.0003
SM	0.034 ± 0.0004	0.040 ± 0.0005	0.068 ± 0.0012	0.081 ± 0.0008	0.010 ± 0.0008
MEI	−0.007 ± 0.0003	−0.041 ± 0.0012	−0.039 ± 0.0010	−0.007 ± 0.0002	−0.006 ± 0.0003
TSI	−0.007 ± 0.0002	−0.012 ± 0.0014	−0.0004 ± 0.0001	−0.003 ± 0.0002	−0.003 ± 0.0002
Model (all predictors)	0.335 ± 0.0030	0.212 ± 0.0038	0.117 ± 0.0027	0.253 ± 0.0022	0.121 ± 0.0020
Observed	0.384	0.274	0.157	0.288	0.154

WMGHG well-mixed Greenhouse Gases radiative forcing, SM near-surface Soil Moisture, AOD aerosol optical depth, MEI multivariate, El Niño/Southern Oscillation Index, TSI total solar irradiance), determined from the slopes of the linear models (e.g., Fig. 4b–f). (Units: °C per decade).

nearly half (33–45%) of the observed temperature variability as well as the recent warming trends (Fig. 2 and Table 1). In relative terms, it is found to be highest in two of the Southern Hemispheric MCRs, SAF and SAU (44.9 and 40.7% of the variability, respectively). Land-atmosphere interactions and variability in soil moisture explain a significant fraction of temperature anomalies in all regions. This is most prominent in NAC (28.9% relative contribution to the observed variability), a region that, similarly to the Mediterranean Basin, is subject to pronounced trends of soil aridification (Supplementary Figs. 3, 4) and has experienced multi-year droughts. To demonstrate this feedback, we present composites of summer temperature anomalies during the years with near-surface soil moisture below the 10th and above the 90th percentiles during the period 1981–2020 for NAC and MED (Fig. 3). During the driest years, summers in both regions are up to 3 °C warmer than the long-term mean. A similar analysis for the Southern Hemisphere is presented in Supplementary Fig. 5. In agreement with the relative importance analysis, this feedback is more evident in South American and South African MCRs.

The relative contribution of ENSO, a natural oscillation that can nevertheless be impacted by anthropogenic factors, in the observed temperature variability is significant primarily in the regions adjacent to the Pacific Ocean. Particularly over the American continents, it is found to contribute 13.6% and 19.5% in NAC and SAC, respectively. In these regions, ENSO has

contributed to a cooling of about 0.04 °C per decade or 0.1–0.2 °C during the last 40 years (Table 1). Despite apparent sunspot cycles, solar irradiance (TSI) explains <2% of the observed temperature variability in all regions except in southern Africa (7.5%). The declining trend of TSI (Supplementary Fig. 2) has contributed to decelerating the warming rates, however, this is negligible compared to the other drivers.

Contrary to all other MCRs (relative contribution less than 1%), the influence of aerosol radiative effects (with natural and anthropogenic components) in the Mediterranean Basin has been significant (23% of explained variability), and has been one of the dominant regional drivers of accelerated warming (Table 1). The Mediterranean AOD trends (Supplementary Fig. 6) are primarily negative and are more pronounced during the late spring and summer months. The MED Basin is the only Mediterranean climate-type region globally with statistically significant AOD trends during the past four decades.

Drivers of Mediterranean warming amplification

The outcomes of the statistical model, designed for reconstructing temperature and decomposing its variability components, are presented in Fig. 4a for the Mediterranean Basin, the largest of the regions with Mediterranean climate characteristics, and having experienced the most robust warming acceleration in the period

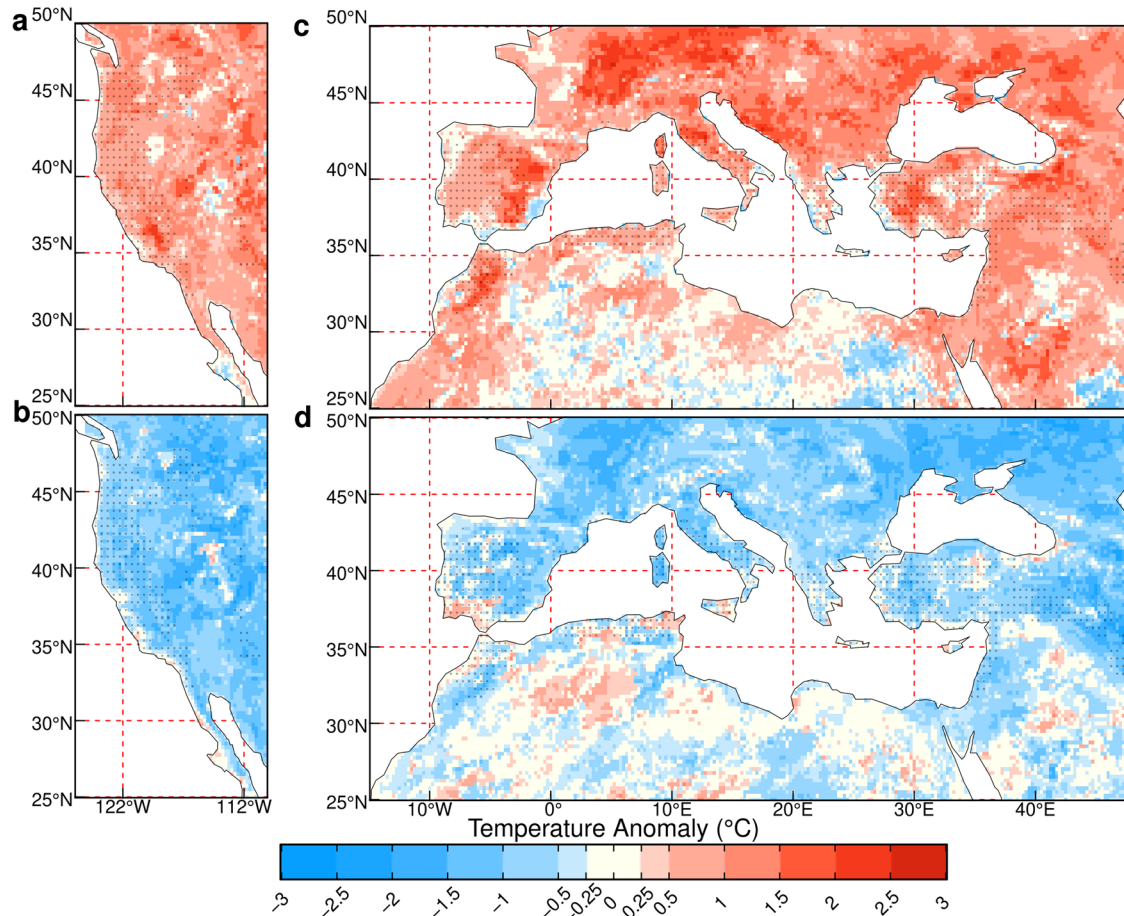


Fig. 3 Composite analysis. Composite analysis of temperature anomalies during the summers with near-surface soil moisture values below the 10th (a, c) and above the 90th (b, d) percentile during 1981–2020, for North America—California (NAC, left panels) and the Mediterranean Basin (MED, right panels). Stippling indicates the regions with a Mediterranean climate type.

1981–2020. Similar results for the other MCR regions are presented in Supplementary Figs. 7–10. For all cases, the reconstructions slightly underestimate the observed warming trends; for the MED, this is $0.38\text{ }^{\circ}\text{C}$ per decade (Table 1). The contribution of each climate driver to the observed temperature variability, including the residuals, is presented in Fig. 4b–g, while Table 1 presents a summary of each of the climate drivers.

Overall, the WMGHG radiative forcing dominates the observed trend ($0.18\text{ }^{\circ}\text{C}/\text{decade}$). The contribution of declining AOD is also significant ($0.1\text{ }^{\circ}\text{C}/\text{decade}$). This includes both natural and anthropogenic aerosols and is the combined result of the absence of major volcanic eruptions in the last two decades of the time series, a decline in North African and Middle Eastern dust concentrations, mostly related to natural variability^{43,44}, and a well-documented decrease of anthropogenic aerosols, following the implementation of cleaner air policies by European countries^{45,46}.

Total (natural and anthropogenic) MERRA-2 AOD trends in the broader Mediterranean region are presented in Supplementary Fig. 6. A statistically significant negative trend is evident for most of the area. According to this dataset, in the early part of the record, the contribution of the El Chichón (Mexico, 1982) and Mt. Pinatubo (Philippines, 1991) volcano eruptions to negative temperature anomalies is substantial (Fig. 4c). The potential contribution of decreasing sulfate from anthropogenic sources cannot be established from the particular AOD dataset (MERRA-2), however, it is evident from the ground-based observations at Finokalia station in Crete, Greece (Fig. 5a). This station is considered representative of the eastern Mediterranean environment, where a clear negative sulfate trend of about $-1.2\text{ }\mu\text{g per m}^3$ per decade

has been observed. While this dataset is the longest available in the region, it does not cover the entire period since 1980. Sporadic or non-continuous data collected at other Eastern Mediterranean stations in Greece (e.g., Fig. 5b), Israel, and Cyprus confirm the high sulfate values observed at Finokalia at the beginning of the 1990s and the decreasing trend in the more recent years. They also indicate even higher sulfate levels at the beginning of the 1980s by $\sim 40\%$ compared to the 1990s. For example, in the suburban station of Athens (Fig. 5b), the observed trend for 1980–2008 is $-1.7\text{ }\mu\text{g per m}^3$ per decade. This reduction is more evident in the summer months, coinciding with the higher warming rates compared to the other seasons⁴⁷. In Finokalia, besides the apparent opposite direction of long-term trends for the common period of monthly temperature and sulfate measurements, these two parameters are highly anti-correlated (Spearman correlation coefficient of -0.61). This value is statistically significant at the 99% confidence interval. A statistically significant anti-correlation of -0.7 is also found between temperature and AOD in the Mediterranean Basin (not shown). Such strong anti-correlations are not evident in the other MCRs.

Negative trends of near-surface soil moisture contribute to an observed Mediterranean warming of about $0.04\text{ }^{\circ}\text{C}/\text{decade}$ (Table 1 and Fig. 4d). The temperature trend associated with land-atmosphere interactions has been particularly evident in the last 20 years of our time series. Such interactions, considered also as positive warming feedback, are important in all Mediterranean climate-type regions, particularly in SAC and SAF. In SAC, the warming attributed to this positive feedback is comparable to the

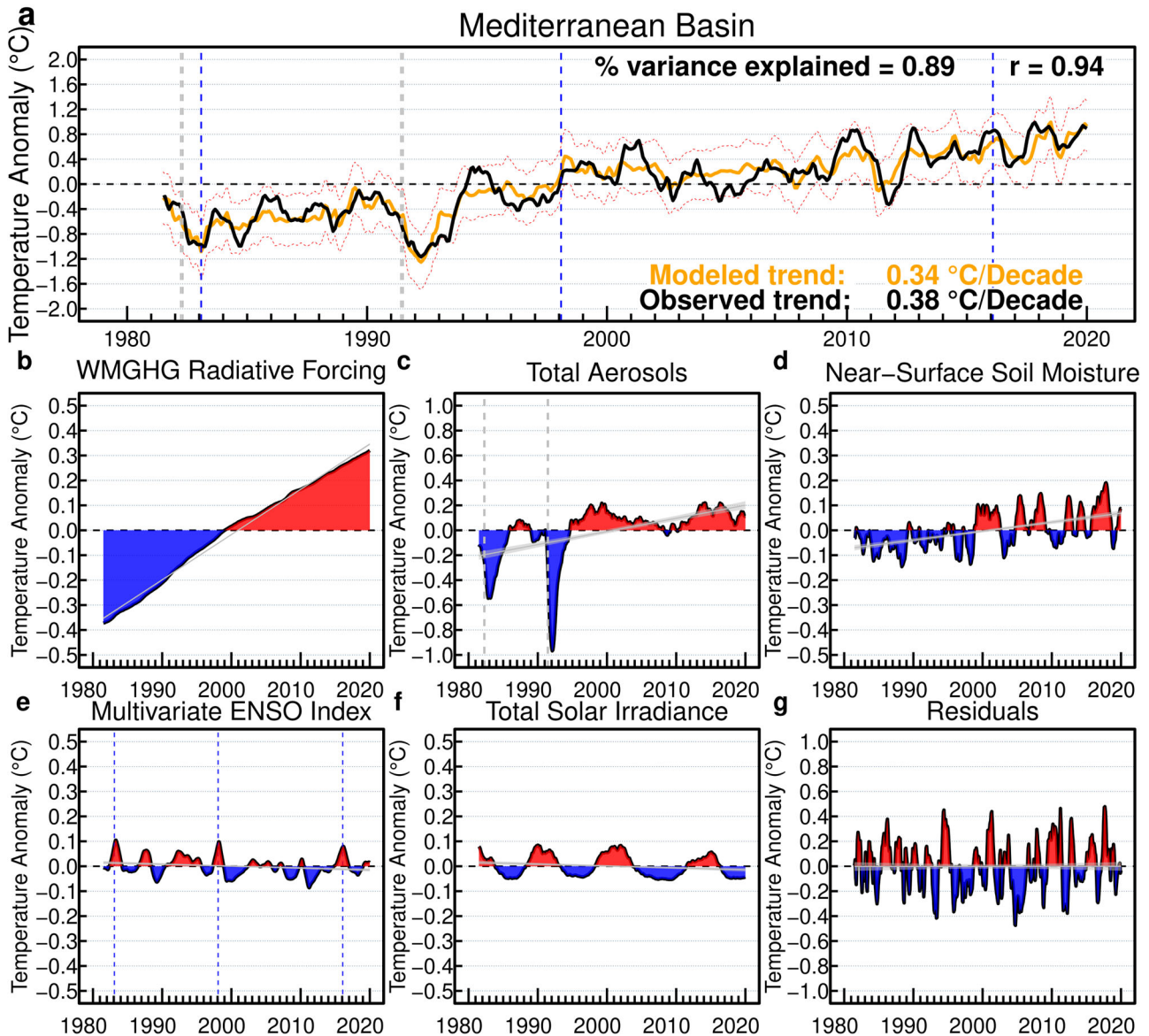


Fig. 4 Decomposed temperature anomalies. **a** Observed (CRU-TS) and reconstructed temperature anomalies, with respect to the 1981–2020 mean value, for the Mediterranean Basin. The correlation coefficient (R) between the two-time series, their linear trends, and the percentage of explained variance are also indicated. The light red curves indicate the 95% confidence intervals of the multivariate lagged linear regression model. The vertical dashed lines indicate major volcanic eruptions (gray) and end years of significant El-Niño events (blue). **b–g** Temperature anomalies attributed to well-mixed greenhouse gases' radiative forcing (WMGHG), natural and anthropogenic aerosols (total AOD), El Niño/Southern Oscillation (ENSO), near-surface soil moisture, solar forcing, and residuals. Gray lines in **b–g** are linear model fits the predicted anomalies.

warming due to greenhouse gases (0.07 and 0.08 °C/decade, respectively).

Compared to the other drivers, the effects of internal climate variability (ENSO) and solar activity on the Mediterranean temperature variability is limited (± 0.01 °C) and is driven by natural oscillations (Fig. 4e, f). They both contribute to a deceleration of the observed warming, however, their contribution compared to the other prevailing drivers (e.g., WMGHG, AOD, and SM) is negligible (Table 1).

DISCUSSION

The analysis of temperature trends over the last 120 years underscores that the Mediterranean Basin has been warming more rapidly than the global rate, and of any other MCR region

(defined by similar geographical and climate characteristics), especially during the past four decades (1981–2020). Our temperature reconstruction model captures the observed variability and warming rates. The monotonically increasing radiative forcing of greenhouse gases explains most of the observed warming in all MCRs (0.08–0.18 °C per decade).

We find that the Mediterranean Basin warming amplification is mainly attributed to the combined effect of reduced aerosol optical depth (the second most dominant driver, following the radiative forcing by well-mixed greenhouse gases) and decreasing soil moisture. The declining aerosol optical depth in the Mediterranean region is related to the relatively quiescent volcanic period after major eruptions in the 1980s and 1990s, naturally-induced decreases in North African and Middle Eastern dust influences, in addition to significant decreases in

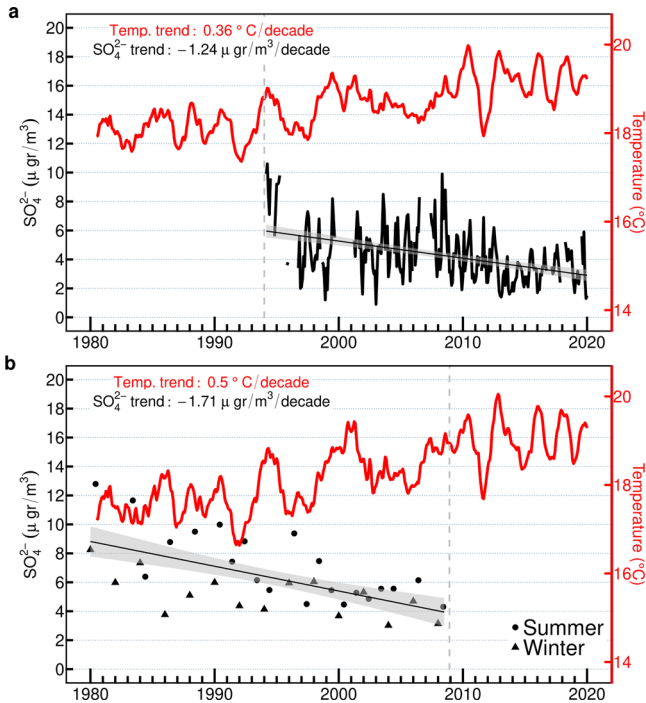


Fig. 5 Aerosol observations in the eastern Mediterranean. Monthly sulfate aerosol (SO_4^{2-}) observations (black points and curve) and temperature time series (red curves) at **a** Finokalia, Crete and **b** Athens in Greece. **b** Winter and summer refers to the average of January–February and June–July months, respectively.

anthropogenic emissions, primarily in central and subsequently in eastern Europe.

Our findings corroborate previous studies based on different approaches. For example, based on sensitivity simulations, aerosol reductions in Europe have contributed $23 \pm 5\%$ to regional warming over the period 1980–2012⁴⁸. The largest decreases in sulfur dioxide emissions and MERRA-2 AOD over Europe occurred in the 1980s and 1990s^{45,46,49}. Atmospheric aerosols have continued to decrease after 2000, although at a substantially slower rate³⁸. Their influence is most evident during the dry and mostly cloud-free summer season, associated with stable atmospheric conditions and predominantly northerly flow that connects the polluted European continent with the Mediterranean. We also find the most significant declines in AOD and SO_4^{2-} concentrations during this season.

In most MCRs, precipitation variability is pronounced and is largely controlled by natural climate oscillations; nevertheless, there is growing evidence that anthropogenic climate change is related to a transition to drier regimes. This is partly due to changes in the general circulation and the poleward expansion of the downward branch of the Hadley cell, also associated with northward shifting storm tracks, mainly during the wet season^{12,50}. In addition, the increasing temperatures, mainly in spring and summer, have contributed to soil moisture depletion through enhanced evapotranspiration⁵¹. In the present analysis, such land-atmosphere interactions explain a large part of the observed temperature variability (up to 29% relative contribution to the observed variance) and significantly add to regional warming. Trends are more pronounced during the spring and summer seasons, contributing to enhanced warming during the already warm or hot part of the year. The attribution of this amplifying feedback to human activities needs to be further investigated since it is strongly linked to both natural (e.g., internal climate variability) and anthropogenic factors (e.g., enhanced warming or

precipitation declines), particularly in Mediterranean-type environments.

Our analysis highlights the important role of aerosols in temperature variability, though with considerable uncertainty, since both direct (through solar radiation extinction) and indirect effects (through interactions with clouds) may be involved²². For example, complex dust-pollution-cloud interactions can reduce the condensed water path and hence the reflection of solar radiation⁵². Such interactions need to be more explicitly considered in attribution studies. Volcanic activity is an important natural cause of climate variability because the accompanying sulfur emissions impact the aerosol optical depth^{34,53}. Volcanic aerosol particles that reach the stratosphere can cool the surface and the troposphere by scattering solar radiation. At the same time, they warm the lower stratosphere, absorbing thermal infrared (IR) and solar near-IR radiation⁵⁴. The climate signal of desert dust, considered to be of natural origin, is not fully understood^{55,56}, and is typically not included in regional climate models. Even though deserts are a main natural source of dust particles, anthropogenic climate change can influence the emission mechanism, for example, through drying of the soils, land-use change or deviations in wind patterns, and the frequency and trajectories of cyclones^{57,58}.

The role of increasing WMGHGs in observed warming is robust and dominant in all regions. Their relative contribution is high in the Southern Hemispheric Mediterranean climate-type regions, also related to the less pronounced trends of other climate drivers. Nevertheless, the absolute contribution of WMGHGs in the Southern Hemisphere warming is overall lower. This is in agreement with previous studies, which highlight that the radiative forcing and consequent net warming are most pronounced in the Northern Hemisphere, even though most greenhouse gases act globally⁵⁹.

The remaining unattributed variability is relatively small but could be addressed further by considering additional drivers, such as radiative forcing of short-lived greenhouse gases (e.g., tropospheric ozone), indicators for land-use changes (e.g., deforestation and urbanization) or sea surface temperature (SST) anomalies. Such analyses are hampered by the dearth of continuous long-term measurements. For example, SST trends are not uniform, and the Mediterranean Sea (mainly in the eastern part) is warming more strongly than the oceans that are adjacent to other MCRs (Supplementary Fig. 11). This is also the case for the Black Sea, which is contiguous to MCRs in Anatolia and is warming at rates greater than 0.5°C per decade. The difference in warming rates compared to the open oceans may be related to the Mediterranean being an enclosed and relatively small basin. Cooling through large-scale upwelling is also more evident in other regions, such as the eastern Pacific Ocean⁶⁰. It was also found that urban areas in the Mediterranean area warm at higher rates than their rural surroundings⁴⁷. We anticipate that urbanization can be included in our model in the near future as long-term measurement data (e.g., from remote sensing) become available.

METHODS

Data and sources of climate drivers

To analyze temperature trends and variability, we used gridded observations from the CRU-TS v4.05 dataset⁶¹, available globally at a spatial resolution of $0.5^\circ \times 0.5^\circ$. We derived monthly anomalies (land-only, area-weighted means) over the period 1981–2020. For assessing the significance of trends, we have used the non-parametric Mann-Kendall test⁶². We consider the trends with p-values lower than 0.05 to be statistically significant.

The Mediterranean climate-type zones (Fig. 2) were calculated according to the Köppen–Geiger climate classification³. Annual means of temperature and precipitation (derived from CRU-TS

v4.05), as well as their extreme monthly values and seasonality, were assessed. The warm temperate, dry summer climate zones with hot (Csa) and warm summer conditions (Csb) are considered Mediterranean type¹.

For the Total Solar Irradiance (TSI), we used a composite record compiled from measurements made by independent space-based radiometers from 1978 onwards^{63,64}.

For the well-mixed greenhouse gases (WMGHGs), we used globally averaged carbon dioxide (CO₂), methane (CH₄), nitrous oxide (N₂O), and trichlorofluoromethane (CFC-11 and CFC-12) concentrations derived from NOAA's Global Monitoring Laboratory (<https://gml.noaa.gov/>). To calculate the monthly WMGHG radiative forcing, we followed the methodology of Hofmann et al.⁶⁵. Although the selected GHGs are relatively well-mixed throughout the atmosphere, and most climate simulations are based on a globally uniform or latitudinally-resolved concentrations assumption, satellite observations reveal a non-uniform distribution of GHG concentrations (e.g., atmospheric CO₂)³¹. Therefore, we have scaled the global time series to the different regions by using spatial information provided by Cheng et al.³¹. Other greenhouse gases (e.g., ozone—O₃ or hydrochlorofluorocarbons—HCFCs) were not included in the analysis since the mathematical expressions for calculating their radiative forcing were not available in Hofmann et al.⁶⁵.

Near-surface soil moisture, used to assess land-atmosphere temperature coupling, is derived from the ERA5 reanalysis data⁶⁶, available from the Copernicus Climate Change Service (C3S) Climate Data Store (<https://cds.climate.copernicus.eu>) at a spatial resolution of 30 km. We used monthly mean values for the soil level nearest to the surface (<7 cm). Sea surface temperature was also derived from the ERA5 reanalysis.

The El Niño/Southern Oscillation (ENSO), a naturally occurring anomalous state of tropical Pacific coupled ocean-atmosphere conditions, is utilized as a predictor representing global natural climate variability. We applied the bi-monthly Multivariate El Niño/Southern Oscillation Index (MEI.v2), which combines both oceanic and atmospheric variables and facilitates in a single index an assessment of ENSO⁶⁷. In particular, it provides real-time indications of ENSO intensity and, through historical analysis, a context for meaningful comparative studies of evolving conditions.

For the aerosol radiative forcing, we used total Aerosol Optical Depth (AOD) data from the Modern-Era Retrospective analysis for Research and Applications version 2 (MERRA-2). MERRA-2 is the latest version of the global atmospheric reanalysis of satellite products by the NASA Global Modeling and Assimilation Office (GMAO) using the Goddard Earth Observing System Model (GEOS).

In addition to the MERRA-2 data, sulfate (SO₄²⁻) aerosol observations are obtained from two monitoring sites in Greece (Finokalia and Athens). The atmospheric research station of the University of Crete has been operating on the northern coast of Crete at Finokalia (35.33°N, 25.66°E) since 1993. It is located at the top of a hill (250 m above sea level) facing the sea within a sector of 270° to 90°. No significant human activities occur at a distance closer than 15 km within the above-mentioned sector. The Athens urban background monitoring station for aerosol properties is operated by the National Center for Scientific Research "Demokritos". It lies 7 km North East of the historic city center of Athens on the hillside of Hymettus Mountain (37.98°N, 22.19°E, 270 m above sea level). It is located in a vegetated area with suburban characteristics.

Multivariate lagged linear regression model

To explore the role of each driver, we use a mathematical reconstruction model of temperature^{35,68–71}. We assessed the relative importance (contribution) of each variable for the 1981–2020 monthly surface temperature in all regions with Mediterranean climate type. The reconstruction of temperature

time series (T_R) has been derived from normalized (zero-mean, unit-variance) time series of well-mixed greenhouse gases radiative forcing (WMGHG), total solar irradiance (TSI), total aerosol optical depth (AOD), Multivariate El Niño/Southern Oscillation Index (MEI), and near-surface soil moisture (SM). Before feeding the temperature reconstruction model, we decomposed the monthly time series of temperature and each predictor (climate driver) to remove seasonality.

We fitted a multivariate lagged linear regression of regional temperature time series for each MCR. Since there is a memory effect involved in some of the temperature drivers^{35,42,69}, we applied different time lags (Δt) chosen to maximize the explained variance using a two-way interaction approach. The following time lags (Δt in months) were used: $\Delta t_{\text{WMGHG}} = 120$, $\Delta t_{\text{SM0}} = 0$, $\Delta t_{\text{SM4}} = 4$, $\Delta t_{\text{AOD0}} = 0$, $\Delta t_{\text{AOD4}} = 4$, $\Delta t_{\text{MEI2}} = 2$, $\Delta t_{\text{MEI4}} = 4$, $\Delta t_{\text{TSI}} = 1$. These lags are found to maximize the explained variance considering a range of thermal inertia involved in critical climate processes. The reconstructed temperature time series (T_R) in each MCR were estimated according to Eq. (1):

$$T_{R(t)} = b_0 + b_1 \text{WMGHG}_{(\Delta t_{\text{WMGHG}})} + b_2 \text{SM}_{(\Delta t_{\text{SM0}})} + b_3 \text{SM}_{(\Delta t_{\text{SM4}})} + b_4 \text{AOD}_{(\Delta t_{\text{AOD0}})} + b_5 \text{AOD}_{(\Delta t_{\text{AOD4}})} + b_6 \text{MEI}_{(\Delta t_{\text{MEI2}})} + b_7 \text{MEI}_{(\Delta t_{\text{MEI4}})} + b_8 \text{TSI}_{(\Delta t_{\text{TSI}})} + \text{Interactions} + \epsilon_{(t)} \quad (1)$$

where b_i are the regression coefficients, the interactions term is the summed effect of all two-way interactions among the predictors, and the $\epsilon_{(t)}$ are the model residuals, which represent the unexplained variance.

The relative importance of variables in regression analyses has been widely used in various applications, including the financial and social sciences, epidemiology, but also environmental sciences, and ecology⁷². Here, we utilized a generally applied method for decomposing the model variance, or equivalently, the coefficient of determination (R^2) in the regression analysis. In particular, LMG (from Lindeman, Merenda, and Gold) is based on an unweighted average of sequential explained variances over all possible orderings of regressors⁷².

To obtain uncertainty estimates of the multivariate lagged regression model and relative importance of individual climate drivers we applied a bootstrap approach⁷³. Specifically, we re-sampled with replacement (1000 iterations) the 40-year monthly time series and then refit the model to the resulting time series. This bootstrapping approach robustly quantifies sampling uncertainty in the estimation of the coefficients b_i , which is, in turn, propagated in estimates of T_R (Eq. 1, left-hand side) and thus the relative importance. This is presented in the form of uncertainty intervals (interquartile range).

The estimation of linear temporal trends and associated uncertainty is based on the well-established linear regression theory⁷⁴. Confidence intervals were calculated to demonstrate the uncertainty that is a fundamental aspect of linear regression models. We obtained an interval with a lower and upper bound that is likely to contain the true slope estimate with a 95% level of confidence.

DATA AVAILABILITY

All data used in the present analysis are open-access. More details, sources, and hyperlinks for data access are provided in the Methods section.

CODE AVAILABILITY

The R package "relaimpo" was used to extract the relative importance of the different climate predictors. The R package "purr" was used for bootstrapping in trend analysis. The codes that support the findings of this study are available from the corresponding author upon request.

Received: 7 March 2023; Accepted: 5 July 2023;

Published online: 20 July 2023

REFERENCES

- Seager, R. et al. Climate variability and change of Mediterranean-type climates. *J. Clim.* **32**, 2887–2915 (2019).
- Kottek, M., Grieser, J., Beck, C., Rudolf, B. & Rubel, F. World map of the Köppen-Geiger climate classification updated. *Meteorol. Zeitschrift* **15**, 259–263 (2006).
- Beck, H. E. et al. Present and future köppen-geiger climate classification maps at 1-km resolution. *Sci. Data* **5**, 1–12 (2018).
- Myers, N., Mittermeier, R. A., Mittermeier, C. G., Fonseca, G. A. B. & Kent, J. Biodiversity hotspots for conservation priorities. *Nature* **403**, 853–858 (2000).
- Vogiatzakis, I. N., Mannion, A. M. & Sarris, D. Mediterranean island biodiversity and climate change: the last 10,000 years and the future. *Biodivers. Conserv.* **25**, 2597–2627 (2016).
- Vogel, M. M., Hauser, M. & Seneviratne, S. I. Projected changes in hot, dry and wet extreme events' clusters in CMIP6 multi-model ensemble. *Environ. Res. Lett.* **15**, 094021 (2020).
- Cramer, W. et al. Climate change and interconnected risks to sustainable development in the Mediterranean. *Nat. Clim. Chang.* **8**, 972–980 (2018).
- Peleg, N., Bartov, M. & Morin, E. CMIP5-predicted climate shifts over the East Mediterranean: implications for the transition region between Mediterranean and semi-arid climates. *Int. J. Climatol.* **35**, 2144–2153 (2015).
- Cos, J. et al. The mediterranean climate change hotspot in the CMIP5 and CMIP6 projections. *Earth Syst. Dyn.* **13**, 321–340 (2022).
- Zittis, G. et al. Climate change and weather extremes in the Eastern Mediterranean and Middle East. *Rev. Geophys.* **60**, e2021RG000762 (2022).
- Feng, X., Qian, C. & Matera, S. Amplification of the temperature seasonality in the mediterranean region under anthropogenic climate change. *Geophys. Res. Lett.* **49**, 1–10 (2022).
- Cherif, S. et al. Drivers of change. In: *Climate and Environmental Change in the Mediterranean Basin—Current Situation and Risks for the Future*. First Mediterranean Assessment Report, 59–180 (Union for the Mediterranean, Plan Bleu, UNEP/MAP, 2020).
- Oertel, M., Meza, F. J. & Gironás, J. Observed trends and relationships between ENSO and standardized hydrometeorological drought indices in central Chile. *Hydrol. Process.* **34**, 159–174 (2020).
- Wolski, P. How severe is Cape Town's "Day Zero" drought? *Significance* **15**, 24–27 (2018).
- Gudmundsson, L., Leonard, M., Do, H. X., Westra, S. & Seneviratne, S. I. Observed trends in global indicators of mean and extreme streamflow. *Geophys. Res. Lett.* **46**, 756–766 (2019).
- Zittis, G. Observed rainfall trends and precipitation uncertainty in the vicinity of the Mediterranean, Middle East and North Africa. *Theor. Appl. Climatol.* **134**, 1207–1230 (2018).
- Delworth, T. L. & Zeng, F. Regional rainfall decline in Australia attributed to anthropogenic greenhouse gases and ozone levels. *Nat. Geosci.* **7**, 583–587 (2014).
- Williams, A. P. et al. Contribution of anthropogenic warming to California drought during 2012–2014. *Geophys. Res. Lett.* **42**, 6819–6828 (2015).
- Diffenbaugh, N. S., Swain, D. L., Touma, D. & Lubchenko, J. Anthropogenic warming has increased drought risk in California. *Proc. Natl. Acad. Sci. USA* **112**, 3931–3936 (2015).
- Cook, B. I., Anchukaitis, K. J., Touchan, R., Meko, D. M. & Cook, E. R. Spatiotemporal drought variability in the Mediterranean over the last 900 years. *J. Geophys. Res.* **121**, 2060–2074 (2016).
- Deitch, M., Sapundjic, M. & Feirer, S. Characterizing precipitation variability and trends in the World's Mediterranean-climate areas. *Water* **9**, 259, 1–21 (2017).
- IPCC. Summary for Policymakers. In: *Climate Change 2021: The Physical Science Basis*. Contribution of Working Group I to the Sixth Assessment Report of the Intergovernmental Panel on Climate Change, 3–32, (Cambridge University Press, 2021).
- Zittis, G., Hadjinicolaou, P., Klangidou, M., Proestos, Y. & Lelieveld, J. A multi-model, multi-scenario, and multi-domain analysis of regional climate projections for the Mediterranean. *Reg. Environ. Chang.* **19**, 2621–2635 (2019).
- Spinoni, J. et al. Global exposure of population and land-use to meteorological droughts under different warming levels and SSPs: a CORDEX-based study. *Int. J. Climatol.* **41**, 6825–6853 (2021).
- Spinoni, J. et al. Future global meteorological drought hot spots: a study based on CORDEX data. *J. Clim.* **33**, 3635–3661 (2020).
- Lionello, P. & Scarascia, L. The relation between climate change in the Mediterranean region and global warming. *Reg. Environ. Chang.* **18**, 1481–1493 (2018).
- Almazroui, M. et al. Projected changes in climate extremes using CMIP6 simulations over SREX regions. *Earth Syst. Environ.* **5**, 481–497 (2021).
- Giorgi, F. Climate change hot-spots. *Geophys. Res. Lett.* **33**, L08707 (2006).
- Tuel, A. & Eltahir, E. A. B. Why is the mediterranean a climate change hot spot? *J. Clim.* **33**, 5829–5843 (2020).
- Evan, A. T., Vimont, D. J., Heidinger, A. K., Kossin, J. P. & Bennartz, R. The role of aerosols in the evolution of North Atlantic Ocean temperature anomalies. *Science* **324**, 778–781 (2009).
- Cheng, W. et al. Global monthly gridded atmospheric carbon dioxide concentrations under the historical and future scenarios. *Sci. Data* **9**, 1–13 (2022).
- Mao, K. B. et al. Global aerosol change in the last decade: an analysis based on MODIS data. *Atmos. Environ.* **94**, 680–686 (2014).
- Predybaylo, E., Stenchikov, G. L., Wittenberg, A. T. & Zeng, F. Impacts of a pinatubo-size volcanic eruption on ENSO. *J. Geophys. Res.* **122**, 925–947 (2017).
- Stenchikov, G. The role of volcanic activity in climate and global changes. In: *Climate Change: Observed Impacts on Planet Earth*, 607–643. (Elsevier B.V., 2021).
- Lean, J. L. & Rind, D. H. How natural and anthropogenic influences alter global and regional surface temperatures: 1889 to 2006. *Geophys. Res. Lett.* **35**, L18701 (2008).
- Seneviratne, S. I. et al. Investigating soil moisture-climate interactions in a changing climate: a review. *Earth-Sci. Rev.* **99**, 125–161 (2010).
- Tett, S. F. B. et al. Estimation of natural and anthropogenic contributions to twentieth century temperature change. *J. Geophys. Res. Atmos.* **107**, ACL 10-1–ACL 10-24 (2002).
- Glantz, P., Fawole, O. G., Ström, J., Wild, M. & Noone, K. J. Unmasking the effects of aerosols on greenhouse warming over Europe. *J. Geophys. Res. Atmos.* **127**, e2021JD035889 (2022).
- Stott, P. A. Attribution of regional-scale temperature changes to anthropogenic and natural causes. *Geophys. Res. Lett.* **30**, 1–4 (2003).
- Stern, D. I. & Kaufmann, R. K. Anthropogenic and natural causes of climate change. *Clim. Change* **122**, 257–269 (2014).
- Imbers, J., Lopez, A., Huntingford, C. & Allen, M. R. Testing the robustness of the anthropogenic climate change detection statements using different empirical models. *J. Geophys. Res. Atmos.* **118**, 3192–3199 (2013).
- Folland, C. K., Boucher, O., Colman, A. & Parker, D. E. Causes of irregularities in trends of global mean surface temperature since the late 19th century. *Sci. Adv.* **4**, eaao5297 (2018).
- Shao, Y., Klose, M. & Wyrwoll, K. H. Recent global dust trend and connections to climate forcing. *J. Geophys. Res. Atmos.* **118**, 11,107–11,118 (2013).
- Pikridas, M. et al. Spatial and temporal (short and long-term) variability of sub-micron, fine and sub-10 Mm particulate matter (PM1, PM2.5, PM10) in Cyprus. *Atmos. Environ.* **191**, 79–93 (2018).
- Klimont, Z., Smith, S. J. & Cofala, J. The last decade of global anthropogenic sulfur dioxide: 2000–11 emissions. *Environ. Res. Lett.* **8**, 014003 (2013).
- Cherian, R. & Quaas, J. Trends in AOD, clouds, and cloud radiative effects in satellite data and cmip5 and cmip6 model simulations over aerosol source regions. *Geophys. Res. Lett.* **47**, e2020GL087132 (2020).
- Hadjinicolaou, P., Tzyrkalli, A., Zittis, G. & Lelieveld, J. Urbanisation and geographical signatures in observed air temperature station trends over the Mediterranean and the Middle East-North Africa. *Earth Syst. Environ.* <https://doi.org/10.1007/s41748-023-00348-y> (2023).
- Nabat, P., Somot, S., Mallet, M., Sanchez-Lorenzo, A. & Wild, M. Contribution of anthropogenic sulfate aerosols to the changing Euro-Mediterranean climate since 1980. *Geophys. Res. Lett.* **41**, 5605–5611 (2014).
- Lelieveld, J. et al. Global air pollution crossroads over the Mediterranean. *Science* **298**, 5594, 794–799 (2002).
- Lelieveld, J. et al. Climate change and impacts in the Eastern Mediterranean and the Middle East. *Clim. Change* **114**, 667–687 (2012).
- Zittis, G., Hadjinicolaou, P. & Lelieveld, J. Role of soil moisture in the amplification of climate warming in the eastern Mediterranean and the Middle East. *Clim. Res.* **59**, 27–37 (2014).
- Klingmüller, K., Karydis, V. A., Bacer, S., Stenchikov, G. L. & Lelieveld, J. Weaker cooling by aerosols due to dust-pollution interactions. *Atmos. Chem. Phys.* **20**, 15285–15295 (2020).
- Osipov, S. & Stenchikov, G. Regional effects of the mount pinatubo eruption on the middle east and the red sea. *J. Geophys. Res. Ocean.* **122**, 8894–8912 (2017).
- Stenchikov, G. L. et al. Radiative forcing from the 1991 Mount Pinatubo volcanic eruption. *J. Geophys. Res. Atmos.* **103**, 13837–13857 (1998).
- Hansell, R. A. et al. An assessment of the surface longwave direct radiative effect of airborne dust in Zhangye, China, during the Asian Monsoon Years field experiment (2008). *J. Geophys. Res. Atmos.* **117**, 1–16 (2012).
- Osipov, S. & Stenchikov, G. Simulating the regional impact of dust on the middle east climate and the red sea. *J. Geophys. Res. Ocean.* **123**, 1032–1047 (2018).
- Klingmüller, K., Pozzer, A., Metzger, S., Stenchikov, G. L. & Lelieveld, J. Aerosol optical depth trend over the Middle East. *Atmos. Chem. Phys.* **16**, 5063–5073 (2016).
- Flaounas, E. et al. Mediterranean cyclones: current knowledge and open questions on dynamics, prediction, climatology and impacts. *Weather Clim. Dyn.* **3**, 173–208 (2022).

59. Lelieveld, J. et al. Effects of fossil fuel and total anthropogenic emission removal on public health and climate. *PNAS* **116**, 7192–7197 (2019).
60. Burger, F., Brock, B. & Montecinos, A. Seasonal and elevational contrasts in temperature trends in Central Chile between 1979 and 2015. *Glob. Planet. Change* **162**, 136–147 (2018).
61. Harris, I., Osborn, T. J., Jones, P. & Lister, D. Version 4 of the CRU TS monthly high-resolution gridded multivariate climate dataset. *Sci. Data* **7**, 1–18 (2020).
62. Mann, H. B. Nonparametric tests against trend. *Econometrica* **13**, 245–259 (1945).
63. Fröhlich, C. Solar irradiance variability. *Geophys. Monogr. Ser.* **141**, 97–110 (2004).
64. Fröhlich, C. & Lean, J. The Sun's total irradiance: cycles, trends and related climate change uncertainties since 1976. *Geophys. Res. Lett.* **25**, 4377–4380 (1999).
65. Hofmann, D. J. et al. The role of carbon dioxide in climate forcing from 1979 to 2004: introduction of the Annual Greenhouse Gas Index. *Tellus* **58**, 614–619 (2006).
66. Hersbach, H. et al. The ERA5 global reanalysis. *Q.J.R. Meteorol. Soc.* **146**, 1999–2049 (2020).
67. Wolter, K. & Timlin, M. S. El Niño/southern oscillation behaviour since 1871 as diagnosed in an extended multivariate ENSO index (MEIext). *Int. J. Climatol.* **31**, 1074–1087 (2011).
68. Vogel, M. M. et al. Regional amplification of projected changes in extreme temperatures strongly controlled by soil moisture-temperature feedbacks. *Geophys. Res. Lett.* **44**, 1511–1519 (2017).
69. Lean, J. L. & Rind, D. H. How will Earth's surface temperature change in future decades? *Geophys. Res. Lett.* **36**, 1–5 (2009).
70. Huber, M. & Knutti, R. Natural variability, radiative forcing and climate response in the recent hiatus reconciled. *Nat. Geosci.* **7**, 651–656 (2014).
71. Marotzke, J. & Forster, P. M. Forcing, feedback and internal variability in global temperature trends. *Nature* **517**, 565–570 (2015).
72. Grömping, U. Variable importance in regression models. *Wiley Interdiscip. Rev. Comput. Stat.* **7**, 137–152 (2015).
73. Davison, A. C. & Hinkley, D. V. *Bootstrap Methods and Their Application*. Vol. 1 of *Cambridge Series in Statistical and Probabilistic Mathematics*, (Cambridge University Press, 1997).
74. Faraway J. J. *Linear Models with R*. 2nd edn. (CRC Press, 2014).

ACKNOWLEDGEMENTS

This research was supported by the EMME-CARE project that has received funding from the European Union's Horizon 2020 Research and Innovation Program, under Grant Agreement no. 856612, as well as matching co-funding by the Government of Cyprus. N.M. and M.K. acknowledge support by the Action titled "National Network on Climate Change and its Impacts (CLIMPACT)" which is implemented under sub-project 3 of the project "Infrastructure of national research networks in the Fields of Precision Medicine, Quantum Technology and Climate Change", funded by the Public Investment Program of Greece, General Secretary of Research and Technology/Ministry of Development and Investments. The authors wish to thank Dr. P. Zampas for providing SO_4^{2-} data from Athens and Dr. K. Eleftheriadis for providing filters for ion analysis.

AUTHOR CONTRIBUTIONS

D.U.F. and G.Z. have equally contributed as first authors. D.U.F., G.Z., P.H., and N.M. conceived and designed the project. G.Z., D.U.F., and J.L. led manuscript writing. D.U.F., G.Z., S.O., and M.K. analyzed the data. D.U.F., G.Z., S.O., K.K., M.K., and T.E. contributed materials/analysis tools. All authors interpreted the results. All authors assisted in manuscript writing and preparation. J.L. supervised the project.

FUNDING

Open Access funding enabled and organized by Projekt DEAL.

COMPETING INTERESTS

The authors declare no competing interests.

ADDITIONAL INFORMATION

Supplementary information The online version contains supplementary material available at <https://doi.org/10.1038/s41612-023-00423-1>.

Correspondence and requests for materials should be addressed to George Zittis or Jos Lelieveld.

Reprints and permission information is available at <http://www.nature.com/reprints>

Publisher's note Springer Nature remains neutral with regard to jurisdictional claims in published maps and institutional affiliations.



Open Access This article is licensed under a Creative Commons Attribution 4.0 International License, which permits use, sharing, adaptation, distribution and reproduction in any medium or format, as long as you give appropriate credit to the original author(s) and the source, provide a link to the Creative Commons license, and indicate if changes were made. The images or other third party material in this article are included in the article's Creative Commons license, unless indicated otherwise in a credit line to the material. If material is not included in the article's Creative Commons license and your intended use is not permitted by statutory regulation or exceeds the permitted use, you will need to obtain permission directly from the copyright holder. To view a copy of this license, visit <http://creativecommons.org/licenses/by/4.0/>.

© The Author(s) 2023